

Research Articles | Systems/Circuits

Response of neuronal populations to phase-locked stimulation: model-based predictions and validation

<https://doi.org/10.1523/JNEUROSCI.2269-24.2025>

Received: 9 December 2024

Revised: 6 February 2025

Accepted: 1 March 2025

Copyright © 2025 Mirkhani et al.

This is an open-access article distributed under the terms of the [Creative Commons Attribution 4.0 International license](#), which permits unrestricted use, distribution and reproduction in any medium provided that the original work is properly attributed.

This Early Release article has been peer reviewed and accepted, but has not been through the composition and copyediting processes. The final version may differ slightly in style or formatting and will contain links to any extended data.

Alerts: Sign up at www.jneurosci.org/alerts to receive customized email alerts when the fully formatted version of this article is published.

1 Title: Response of neuronal populations to phase-locked
2 stimulation: model-based predictions and validation
3

4 Abbreviated title: Validating modelled neural response to stimulation
5

6 Nima Mirkhani^{1*}, Colin G. McNamara^{1,2}, Gaspard Oliviers¹, Andrew Sharott¹, Benoit Duchet¹,
7 Rafal Bogacz¹
8

9 ¹ MRC Brain Network Dynamics Unit, Nuffield Department of Clinical Neurosciences, University
10 of Oxford, Oxford OX1 3TH, UK

11 ² University College Cork, Cork T12 K8AF, Ireland
12

13 * Corresponding author. E-mail address: nima.mirkhani@ndcn.ox.ac.uk
14

15 Number of pages: 35

16 Number of figures: 6
17

18 Number of words:

19 Abstract: 230

20 Introduction: 684

21 Discussion: 1309
22

23 **Declaration of Competing Interest**

24 C.G.M. and A.S. are inventors on a pending patent application related to the subject matter of this
25 paper.

26 **Acknowledgments**

27 The authors would like to acknowledge the use of the University of Oxford Advanced Research
28 Computing (ARC) facility in carrying out this work. <http://dx.doi.org/10.5281/zenodo.22558>

29 N.M. and R.B. were supported by Medical Research Council Grant MC_UU_00003/1. C.G.M. was
30 supported by the Wellcome Trust (Sir Henry Wellcome Fellowship 209120/Z/17/Z). A.S. and
31 C.G.M. were supported by Medical Research Council Grant MC_UU_00003/6. B.D. was jointly

32 supported by the Royal Academy of Engineering and Rosetrees Trust under the Research
33 Fellowship programme.

JNeurosci Accepted Manuscript

34 Abstract

35 Modulation of neuronal oscillations holds promise for the treatment of neurological disorders.
36 Nonetheless, conventional stimulation in a continuous open-loop manner can lead to side effects
37 and suboptimal efficiency. Closed-loop strategies such as phase-locked stimulation aim to
38 address these shortcomings by offering a more targeted modulation. While theories have been
39 developed to understand the neural response to stimulation, their predictions have not been
40 thoroughly tested using experimental data. Using a mechanistic coupled oscillator model, we
41 elaborate on two key predictions describing the response to stimulation as a function of the phase
42 and amplitude of ongoing neural activity. To investigate these predictions, we analyze
43 electrocorticogram recordings from a previously conducted study in Parkinsonian rats, and extract
44 the corresponding phase and response curves. We demonstrate that the amplitude response to
45 stimulation is strongly correlated to the derivative of the phase response ($\rho > 0.8$) in all animals
46 except one, thereby validating a key model prediction. The second prediction postulates that the
47 stimulation becomes ineffective when the network synchrony is high, a trend that appeared
48 missing in the data. Our analysis explains this discrepancy by showing that the neural populations
49 in Parkinsonian rats did not reach the level of synchrony for which the theory would predict
50 ineffective stimulation. Our results highlight the potential of fine-tuning stimulation paradigms
51 informed by mathematical models that consider both the ongoing phase and amplitude of the
52 targeted neural oscillation.

53

54 Significance Statement

55 This study validates a mathematical model of coupled oscillators in predicting the response of
56 neural activity to stimulation for the first time. Our findings also offer further insights beyond this
57 validation. For instance, the demonstrated correlation between phase response and amplitude
58 response is indeed a key theoretical concept within a subset of mathematical models. This
59 prediction can bring about clinical implications in terms of predictive power for manipulation of
60 neural activity. Additionally, while phase dependence in modulation has been previously studied,
61 we propose a general framework for studying amplitude dependence as well. Lastly, our study
62 reconciles the seemingly contradictory views of pathologic hypersynchrony and theoretical low
63 synchrony in Parkinson's disease.

64

JNeurosci Accepted Manuscript

65

1. Introduction

66 Application of brain stimulation techniques has gained momentum over the past few decades
67 owing to their therapeutic potential (Lozano et al., 2019; Krauss et al., 2021). Neural oscillations
68 can act as anchor points in modulation of brain circuitry (Bergmann and Hartwigsen, 2021;
69 Sullivan et al., 2021). The association of particular network oscillations with different brain
70 functions, as well as their implication in many neurological and psychiatric disorders, renders them
71 suitable targets for stimulation (Strüber and Herrmann, 2020; Oswal et al., 2021; Basu et al.,
72 2023; Zaaimi et al., 2023). Successful manipulation of neural oscillations for the desired outcome
73 requires clear answers to where, how, and when to stimulate (Polanía et al., 2018; Cagnan et al.,
74 2019; Hollunder et al., 2022). The first question has been extensively researched to identify the
75 target site based on the engaged networks (Drobisz and Damborská, 2019; Li et al., 2020; Figeo
76 and Mayberg, 2021; Kübler et al., 2021; Rajamani et al., 2024). To address how and when
77 stimulation should be applied, a variety of closed-loop strategies have been proposed, where
78 features of the ongoing oscillation serve as feedback (Brittain et al., 2013; Scangos et al., 2021;
79 Mondragón-González et al., 2024).

80

81 Among closed-loop techniques, phase-locked stimulation has shown promise in achieving a
82 controlled modulation (Brittain et al., 2013; Cagnan et al., 2017; Mansouri et al., 2018; Krugliakova
83 et al., 2024). In this approach, stimulation pulses are triggered at certain phases of the ongoing
84 oscillatory activity. Neuromodulation and plasticity effects obtained through precise timing of the
85 pulses have been shown to be bidirectional (Huerta and Lisman, 1995; Zanos et al., 2018;
86 Nieuwhof et al., 2022; Li et al., 2023). This feature not only results in higher control and in turn
87 more efficient stimulation policies but may also explain the heterogeneity observed in many open-
88 loop stimulation paradigms. Additionally, due to interactions between different brain rhythms

89 through mechanisms such as phase amplitude coupling, phase-based modulation of an activity
90 can bring about cross frequency changes (Salimpour et al., 2022; Duchet and Bogacz, 2024).

91

92 Despite growing interest in phase-locked stimulation, two main bottlenecks of completely different
93 natures have hindered further application of this strategy. Firstly, real-time tracking of signal
94 properties at the resolution of milliseconds is challenging. Thanks to recent technological
95 advancements and developed algorithms, several studies have demonstrated the implementation
96 of such fast brain-machine interactions in rodents (Siegle and Wilson, 2014; McNamara et al.,
97 2022), non-human primates (Escobar Sanabria et al., 2020; Zaaïmi et al., 2023), and humans
98 (Reis et al., 2021; Gordon et al., 2022). Secondly, theoretical understanding of how the state of a
99 network oscillation at the stimulation time, i.e. its phase and amplitude, modulates the response
100 remains incomplete, often resulting in an extensive search during stimulation sessions for the
101 desired effect. There have been several theoretical studies proposing optimal closed-loop policies
102 (Holt et al., 2016; Popovych et al., 2017; Weerasinghe et al., 2019, 2021). However, the
103 predictions made by these studies have not been thoroughly validated with experimental data,
104 severely limiting their applicability.

105

106 Mathematical models based on coupled oscillators are suitable candidates for bridging this gap
107 due to their ability to replicate neural oscillations (Velazquez et al., 2015; Guevara Erra et al.,
108 2017; Weerasinghe et al., 2021; Sermon et al., 2024). The Kuramoto model, in particular, offers
109 a great advantage for studying phase-locked stimulation by adopting a phase-based description
110 of neural oscillators (Brown et al., 2004; Acebrón et al., 2005). Hence, network dynamics can be
111 explicitly modeled as a function of individual oscillator's phases, which evolve over time based on
112 their natural frequencies and mutual interactions. This model expresses the collective behavior of

113 oscillators in terms of a mean phase and network synchrony, directly proportional to the amplitude
114 of oscillations (Weerasinghe et al., 2019). Given the phase (Cagnan et al., 2017; McNamara et
115 al., 2022) and amplitude (Weerasinghe et al., 2019; Hebron et al., 2024) dependence of
116 stimulation effects, predicting the network response as a function of these two quantities
117 potentially provides clinically translatable predictive power, especially for patients suffering from
118 Parkinson’s disease (PD) or essential tremor (ET) (Meidahl et al., 2017; Frey et al., 2022). The
119 gained insight could also pave the way for combining phase-locked stimulation with adaptive
120 stimulation—a strategy based on ongoing amplitude (Tinkhauser et al., 2017; Smyth et al.,
121 2023)—merging the best of both approaches.

122
123 Here, we aim to expand on the predictions introduced in (Weerasinghe et al., 2019) and test them
124 using previously collected experimental data from (McNamara et al., 2022). We review the
125 predictions derived from the reduced (mean-field) Kuramoto model regarding the role of ongoing
126 oscillations’ phase and amplitude in response to stimulation. Each theoretical prediction is tested
127 separately against the electrocorticogram measurements of Parkinsonian rats subjected to
128 phase-locked stimulation. Phase-wise, we first demonstrate a strong correlation between the
129 amplitude response curve (ARC) and the derivative of the phase response curve (PRC).
130 Regarding the role of amplitude, we show using the full model that the largest effects can be
131 attained by stimulation at intermediate values of network synchrony. Below this peak, where most
132 brain networks operate, the response is characterized by a slight drop and relatively stronger
133 amplification compared to suppression. Taken together, these findings bridge the gap between
134 theory and experiments, unveiling an opportunity to manipulate neural activities in the desired
135 direction more reliably.

136 2. Materials and methods

137 To investigate the effects of stimulation, we introduce our modeling approach and describe the
138 previously collected dataset used to validate the model's predictions. We also detail the
139 techniques employed to link theory and experiments.

140 2.1. Modeling framework

141 The Kuramoto model of coupled oscillators was used to model the oscillations arising from the
142 activity of a neuronal population. In this framework, the network dynamics are described through
143 phases that reflect self-sustained oscillations of weakly coupled oscillators (Strogatz, 2000). We
144 employed such a network model to analyze how external stimulation affects the network activity
145 of a population. In this context, neurons or neural microcircuits with periodic behavior can be
146 regarded as oscillators that interact with each other (Weerasinghe et al., 2019), collectively giving
147 rise to the network activity often recorded in experiments as local field potentials (LFPs) or ECoG
148 oscillations (Fig. 1A,B) (Breakspear, 2017; Bick et al., 2020).

149
150 To assess the impact of external stimulation on these networks, one must make an assumption
151 about how individual oscillators respond to stimulation. Neurons may vary in their phase response
152 depending on their type and various regulating factors (Fink et al., 2013; Goldberg et al., 2013;
153 Phillips et al., 2020). We adopted the classic case compatible with the Hodgkin Huxley model,
154 where a spiking neuron exhibits a biphasic response featuring both phase delay and advance
155 regions (Goldberg et al., 2013). This response behavior, known as type II, has been observed
156 experimentally (Netoff et al., 2005; Akam et al., 2012), and characterized by a slow-down region
157 after the spiking during the refractory period and a speed-up region closely before the spiking

158 (Smeal et al., 2010) (Fig. 1C). We used $Z(\theta) = -\sin\theta$ as a simple phase response curve that
159 satisfies these conditions (Fig. 1D,E).

160

161 The Hodgkin-Huxley model used to demonstrate the concept of a biphasic phase response was
162 developed using the original conductance values and rate functions (Hodgkin and Huxley, 1952).

163 The effect of stimulation was incorporated as an injected square pulse of current with a width of
164 50 μs . Numerical simulations were performed in MATLAB using the Euler method with 0.01 ms
165 time steps.

166

167 2.2. Full Kuramoto model

168 Dynamics of a finite number of coupled oscillators with noise are governed by (Sakaguchi, 1988):

169

$$170 \dot{\theta}_i = \omega_i + K/N \sum_j^N \sin(\theta_j - \theta_i) + \xi_i + I(t)Z(\theta_i) \quad \text{for } i=1, \dots, N. \quad (1)$$

171

172 This set of differential equations describes how the phase of each oscillator, θ_i , evolves in time
173 while interacting with other oscillators through a global coupling constant K and subject to external
174 stimulation $I(t)$ and independent white noise ξ_i :

175

$$176 \langle \xi_i(t) \rangle = 0, \langle \xi_i(t) \xi_j(t') \rangle = 2D\delta(t - t')\delta_{ij}, \quad (2)$$

177

178 where D represents noise intensity. δ and δ_{ij} are the delta Dirac and Kronecker delta functions,
179 respectively.

180 To investigate macroscopic properties of these networks, an order parameter is defined as
181 follows:

$$183 \quad r = \frac{1}{N} \sum_j^N e^{i\theta_j} = \rho e^{i\psi}, \quad (3)$$

184
185 which describes the network activity in terms of the level of synchrony, ρ (ranging from 0 to 1),
186 and the mean phase, ψ . It can be shown that the experimentally measured oscillation amplitude
187 is proportional to the value of synchrony (Weerasinghe et al., 2019).

188
189 Numerical simulations were conducted in MATLAB using the Euler-Maruyama method with a time
190 step 0.5 ms to discretize the system in time. We verified convergence of the numerics for this
191 timestep value. The natural frequencies of oscillators were randomly sampled from a Cauchy
192 distribution with a mean frequency of ω_0 and a width of γ . To simulate phase-locked stimulation,
193 conditions similar to those in (McNamara et al., 2022) were applied. In each stimulation block, a
194 target phase was chosen, and a pulse was delivered when the calculated mean phase crossed
195 this target and more than 80 % of a beta cycle had elapsed since the previous pulse.

196

197 2.3. Reduced Kuramoto model

198 In the limit of an infinite number of oscillators and under certain assumptions regarding the
199 distribution of natural frequencies, the collective behaviour of the network can be described in a
200 simpler way solely by the time evolution of the order parameter (Ott and Antonsen, 2008; Bick et
201 al., 2020). The dynamics of the system, assuming $Z(\theta) = -\sin\theta$, are reduced to two differential
202 equations governing the amplitude (synchrony ρ) and mean phase ψ of the network:

203

$$204 \quad \frac{d\rho}{dt} = -\gamma\rho + \frac{K\rho}{2}(1 - \rho^2) + \frac{I(t)}{2}(1 - \rho^2)\cos(\psi), \quad (4)$$

$$205 \quad \frac{d\psi}{dt} = \omega_0 - \frac{I(t)}{2\rho}(1 + \rho^2)\sin(\psi), \quad (5)$$

206

207 where γ represents the width of the natural frequency distribution that is centered around ω_0 . The
208 last terms in the amplitude and phase equations represent the instantaneous population ARC and
209 PRC, respectively. The ARC represents changes in amplitude as a function of the stimulation
210 phase, and the PRC quantifies variation in the mean phase with respect to the stimulation phase.

211

212 In the absence of noise, such networks would reach a steady state condition with fixed values of
213 ρ . However, in real networks, the oscillation amplitude fluctuates due to finite size effects, noise,
214 and changes in coupling resulting from synaptic plasticity. Nonetheless, the reduced model can
215 be seen as a phenomenological platform that provides intuitions and preliminary predictions.
216 Accordingly, we employed this model as the basis for generating predictions, which were then
217 further refined using the full model to partially capture the missing effects in a reduced model.

218

219 2.4. ECoG recording from Parkinsonian rats

220 In order to test the validity of the theoretical predictions, we used electrocorticogram (ECoG)
221 recordings collected from rats in (McNamara et al., 2022). In this study, in brief, rat models of PD
222 were created through unilateral lesions of the dopaminergic neurons in substantia nigra, resulting
223 in pathologically elevated beta activity in the cortico-basal ganglia network. Stimulating electrodes
224 were then implanted in the globus pallidus (GPe), and activity was recorded using ECoG. Using
225 a real time implementation of the phase tracking algorithm “Oscilltrack” (Sharott and McNamara,
226 2022), each subject underwent phase-locked stimulation at eight equally-spaced target phases
227 based on the ongoing beta signal. Each trial was targeted at a specific phase and consisted of
228 10-14 stimulation blocks, each lasting 20 sec and separated by 5-sec off-epochs where no
229 stimulation was applied (Fig. 2A). Full details are presented in (McNamara et al., 2022).

230

231 ECoG recordings were obtained at a sampling rate of 20 kHz. Stimulation artifacts were initially
232 removed by interpolating the signal from the start of the electrical impulse to 1.5 ms after. The
233 resulting signal was then downsampled to 2 kHz using an anti-aliasing filter. A 4th order bandpass
234 Butterworth filter was subsequently applied to the downsampled signal. The Hilbert transform was
235 then used on the filtered signal to extract the envelope amplitude and phase of the beta
236 oscillations.

237

238 2.5. Experimental response curves

239 The primary approach to extract the experimental ARC and PRC was the block-based method, in
240 which the average behavior of the network during each 20-sec on-epoch was compared with the
241 preceding 5-s off-epoch. More specifically, for the block-based ARC, the average Hilbert
242 amplitude, \bar{a} , of the signal in each epoch was calculated, and the difference represented the
243 amplitude change at the corresponding phase (Cagnan et al., 2017; Duchet et al., 2020) (Fig.
244 2B). Evaluating this change for all target phases enabled us to reconstruct the experimental
245 (block-based) ARC for each animal:

246

$$247 \quad ARC_b = \overline{a_{on}} - \overline{a_{off}}. \quad (6)$$

248

249 To calculate the block-based PRC, phase trajectory in the 5-sec off-epoch was used to fit a linear
250 model for the evolution of the unwrapped phase. Using this model, the expected phase of the
251 system under no stimulation at the end of the 20-sec epoch, $\hat{\psi}$, could be estimated. The difference
252 between this estimated unwrapped phase in the absence of stimulation and the actual unwrapped
253 phase, ψ , as a result of the stimulation was then normalized by the number of pulses (N_{pulse}) in
254 the on-epoch (Fig. 2C). This normalized change was calculated for all target phases, similar to
255 the ARC, to establish the (block-based) PRC for each animal:

256

$$257 \quad PRC_b = \frac{\hat{\psi} - \psi}{N_{pulse}}. \quad (7)$$

258

259 Considering the different sites for stimulation (GPe) and recording (cortex), as well as variability
260 across animals, all curves were phase-aligned based on the most suppressive phase for the
261 purpose of group analysis. To examine the relationship between the response curves, the
262 derivative of the PRC with respect to phase was computed using central differencing.

263

264 When quantifying the size of amplitude change under different oscillation amplitudes, the method
265 above averages the oscillation over a relatively long period compared to the beta cycle's time
266 scale. To capture more transient changes in the amplitude, we also employed a pulse-based
267 approach. In this technique, the average amplitude within 10 ms before and after each pulse was
268 used to establish the amplitude response as a function of the pre-pulse amplitude (Fig. 2D).

269

270 A custom MATLAB script was developed to process the experimental recordings and extract the
271 response curves. Statistical tests and additional data visualizations were carried out using Python-
272 based packages. Pearson's correlation coefficients (R) were calculated to assess the relationship
273 between the ARC and the PRC derivative. Statistical significance of phase dependence in
274 individual ARCs and PRCs was examined using one-way analysis of variance (ANOVA). The
275 relationship between the correlation strength R and the resulting p -value from ANOVA was also
276 quantified using the Spearman correlation coefficient (r_s).

277 2.6. Model fitting

278 To test the prediction based on oscillation amplitude, it was necessary to estimate the network
279 parameters that could reproduce relevant features of the ECoG recordings used for this study.
280 An optimization-based model fitting algorithm was developed in MATLAB to fit the finite Kuramoto
281 model to individual subjects. The algorithm received three dynamic features of the signal (Duchet

282 et al., 2020): power spectrum density (PSD) of the signal, probability density function (PDF) of
 283 the envelope amplitude, and PSD of the envelope amplitude (Fig. 2E). These features embed the
 284 statistics of the signal intensity along with the temporal variations of both the signal and its
 285 amplitude (Sermon et al., 2023). It then employed MATLAB's surrogate optimizer (surrogateopt)
 286 with batch update interval 1 to minimize the following error:

287

$$288 \quad f = \frac{1}{3} \left(\frac{\sum(PSD_{Data} - PSD_{Model})^2}{\sum(PSD_{Data} - \overline{PSD_{Data}})^2} + \frac{\sum(envPDF_{Data} - envPDF_{Model})^2}{\sum(envPDF_{Data} - \overline{envPDF_{Data}})^2} + \frac{\sum(envPSD_{Data} - envPSD_{Model})^2}{\sum(envPSD_{Data} - \overline{envPSD_{Data}})^2} \right). \quad (8)$$

289

290 Given the different scale of the measured values and the model network activity, both
 291 experimental and simulated signals were z-scored to ensure comparability. PSDs were calculated
 292 using Welch's method with frequency resolution of 1 Hz (1-sec window length) and 50 % overlap.
 293 The optimization output provided values for four network parameters: mean frequency ω_0 , width
 294 of the distribution γ , coupling constant K , and standard deviation of the noise σ . The maximum
 295 number of function evaluations for the surrogate optimization was set to 500. Network simulations
 296 at each optimization step were carried out with $N = 200$ oscillators which were randomly sampled
 297 from a Cauchy distribution with the mean ω_0 and width γ . Each set of parameters was simulated
 298 10 times to account for different realizations of noise, and the dynamic features from the resulting
 299 signals were averaged to calculate the optimization error.

300

301 A parameter recovery study was also performed using synthetic data to investigate whether the
 302 values obtained from the fitting procedure for individual parameters are separately identifiable
 303 with respect to network behavior. This series of simulations and optimizations were performed

304 with fewer oscillators ($N = 50$) and lower frequency resolution for PSDs to reduce computational
305 cost while still capturing the model's generalizable features.

306

307 3. Results

308 The state of simple oscillatory systems can be summarized by their phase and amplitude (Fig.
309 3A). Hence, a clinically relevant predictive power may arise from studying the response to
310 stimulation as a function of these two quantities tracked from signals of interest (e.g. tremor in ET
311 or beta in PD). We first introduce the predictions made by the reduced model regarding the phase
312 and amplitude dependence of the response to stimulation. We then examine the correlation
313 between the PRC and ARC in the data from Parkinsonian rats. Finally, we compare amplitude-
314 dependence in the experimental response with simulations of the best-fitting Kuramoto models.

315 3.1. Predictions from the reduced model

316 First, we focused on the phase dependence of the response behavior (Fig. 3B). Given a specific
317 phase response function for individual oscillators, the reduced model predicted that the population
318 PRC which represents the phase response of the network mirrors the form of the individual
319 oscillators' response function (Weerasinghe et al., 2019). More importantly, the amplitude
320 response of the population summarized by the ARC will be negatively correlated with the
321 derivative of the PRC. To develop an intuition about this prediction, two extreme scenarios of
322 maximum suppression and maximum amplification can be helpful. In the former case, when
323 stimulating the network at the mean phase of π , the trailing oscillators are in the "slow down"
324 region of their cycle while the leading ones have entered the "speed up" regime (Fig. 3B, left
325 inset). As a result, stimulation enlarges the gap between oscillators, causing a more

326 desynchronized system. Conversely, in the maximum amplification scenario, stimulating at the
327 mean phase of 0 causes leading and trailing oscillators to experience opposite effects, making
328 them more tightly packed and thus synchronized (Fig. 3B, right inset). Hence, the maximum
329 suppression and amplification correspond to phases where the absolute slope of the PRC is the
330 largest.

331

332 Next, we sought to predict the network response in terms of amplitude dependence. In the
333 reduced model, the last term of eq. (4) $(\frac{1}{2}(1 - \rho^2)\cos(\psi))$ describes the instantaneous effect of a
334 stimulation impulse, and the scaling factor of this term $(\frac{1}{2}(1 - \rho^2))$ is plotted in Fig. 3C. This figure
335 illustrates that the attainable absolute change in amplitude from stimulation drops continuously
336 as a function of synchrony in the network. In other words, the theory suggests that stimulation
337 should have the greatest effect when applied at low oscillation amplitudes and becomes less
338 effective at large amplitudes. An intuition for this prediction can be obtained by looking at two
339 ends of the synchrony spectrum. Any change in network synchrony requires differential effects of
340 stimulation on the oscillators which leads to an increased or decreased gap between them. In a
341 network with low synchrony, the high dispersion among oscillators allows for the maximum
342 attainable change as a result of stimulation (Fig. 3C, left inset), whereas in a highly synchronized
343 system, all oscillators experience nearly the same change, leading to minimal impact on the
344 collective synchrony (Fig. 3C, right inset).

345

346 Examining eq. (4) for amplitude in the reduced model, the last term represents the combined
347 effect of phase and amplitude which can be visualized as a 3D surface (Fig. 3D). For a more
348 detailed assessment of the model's predictions, we tested each component separately using the
349 experimental data.

350

351 3.2. Correlation between the PRC derivative and ARC

352 To test the theoretical predictions regarding ARC and PRC, we extracted the corresponding
353 curves from the animal data. Analysis of changes in beta power as a function of target phase in
354 (McNamara et al., 2022), revealed nearly antiphase maximum amplification and suppression in
355 all animals. This general trend suggests that $Z(\theta) = -\sin\theta$ can be viewed as a reasonable
356 assumption for phase response function of individual oscillators (see eq. (1)). Nevertheless, ARC
357 and PRC curves for each animal enabled a more comprehensive analysis of the predictions. The
358 block-based method, described above, was employed to calculate the phase and amplitude
359 changes in the high-beta activity as a function of the phase of stimulation. The average PRC,
360 pooled across all animals, exhibited the previously described “slow down” and “speed up” regions
361 for the population activity (Fig. 4A). The corresponding ARC also confirmed antiphase maximum
362 suppression and amplification with smooth transitions in between (Fig. 4B). More importantly, the
363 core prediction of the model, which posits a correlation between ARC and PRC derivative, was
364 examined by establishing the derivative curve calculated through central differencing (Fig. 4B).
365 Comparing ARC and PRC derivative revealed a negative correlation, in agreement with the
366 model's prediction.

367

368 To further quantify this correlation and its variability across animals, we examined the phase and
369 amplitude responses for 13 individual animals at each of the 8 target phases (individual response
370 curves available in Fig. 4-1). The data across all animals and phases showed a tight distribution
371 around a line with a negative slope, resulting in a high correlation coefficient ($R = 0.84$) which
372 underscored the validity of the predicted relationship (Fig. 4C, individual correlations available in

373 Fig. 4-2). To assess how reliably the amplitude response can be predicted given a specific PRC,
374 the relationship between the correlation strength, R , and the presence of an effect of phase in the
375 PRC was explored. The latter was represented by the p -value from the statistical tests where
376 lower values indicate significant phase dependence in the PRC. Plotting these values for different
377 subjects revealed an interesting trend regarding variability across animals (Fig. 4D). All subjects
378 with statistically significant PRCs exhibited a strong correlation with their amplitude response ($R >$
379 0.8). Notably, the phase response of the only subject lacking this correlation did not reach the
380 significance threshold. Additionally, subjects with a higher effect of phase tended to show stronger
381 correlations ($r_s = -0.71, p = 6.7e - 3$). These results suggest that when certain model
382 assumptions are met, —specifically, when phase dependence is present in the response— a tight
383 correlation between ARC and PRC derivative may yield clinical insights when evaluating
384 stimulation outcomes.

385

386 3.3. Contributing factors in amplitude modulation of the response

387 Following the study of phase dependence, we proceeded with analyzing how the network
388 response is influenced by the ongoing oscillation amplitude. The previously described prediction
389 on the dependence of stimulation effects on the ongoing amplitude (Fig. 3C), was derived from
390 the instantaneous effect of stimulation, i.e. the effect was defined as difference between amplitude
391 of oscillations just after and just before the pulse. However, to understand longer term effects,
392 one needs to also consider the dynamics of the system between the pulses. The changes in the
393 oscillation amplitude in the model are described by eq. (4). It states that the amplitude ρ is not
394 only influenced by the stimulation term but also depends on the coupling K and the distribution
395 width γ , which together determine how amplitude evolves in subsequent time steps. In other

396 words, it is not possible to study the longer-term response as a function of amplitude without
397 considering the intrinsic network parameters. In addition, oscillation amplitude is naturally
398 bounded by the minimum and maximum levels of synchrony ($0 < \rho < 1$).

399

400 To develop an intuition about the interaction of these contributing forces in amplitude modulation,
401 a seesaw analogy can be useful (Fig. 5A). Each position of a seesaw corresponds to a specific
402 balance between two opposing forces: one pushing the system towards synchrony and the other
403 causing desynchronization. Within the Kuramoto framework, intrinsic noise D and width γ of the
404 natural frequency distribution, and external stimulation at phases around the mid-ascending part
405 of the cycle tend to reduce the synchrony of the network, tipping the balance towards lower ρ
406 values (Fig. 5A, top). On the contrary, coupling K in the system and stimulation at phases around
407 the mid-descending part shift the balance in favor of higher ρ values by enhancing the network
408 synchrony (Fig. 5A, top). Furthermore, analogous to a real seesaw that is constrained at both
409 ends, there are lower and upper bounds on how the force imbalance is reflected in the network
410 (Fig. 5A, bottom).

411

412 As mentioned earlier, the introduced Kuramoto model's term for absolute change as a function of
413 oscillation amplitude highlights only the stimulation-induced instantaneous changes in the time
414 evolution of amplitude (Fig. 5B, top), without taking into account network dynamics influenced by
415 intrinsic parameters. The reduced model offers an initial insight into the interaction of these
416 contributing factors. In asynchronous networks (Fig. 5B, left inset), relatively high stimulation-
417 induced perturbations are partially offset by network's tendency to return to its steady-state with
418 a low synchrony during the intervals between the pulses. As the network begins transitioning to a
419 partially synchronized state (Fig. 5B, middle inset), a slight decrease in the effect of individual

420 stimulation pulses emerges, but the network is notably more susceptible to changes, reflected in
421 a smaller decay between pulses, which translates into larger shifts in average network synchrony.
422 Lastly, under substantial levels of synchrony (Fig. 5B, right inset), not only is the stimulation effect
423 diminished, but the network again shows a strong tendency to maintain its steady state, leading
424 to smaller net changes in synchrony. Such variations in network tendencies could be better
425 understood by looking at its characteristic curve (Fig. 5-1).

426

427 To further characterize the absolute change as a function of amplitude and link the model's
428 prediction with the experimental data, evolution of oscillation amplitude within similar stimulation
429 blocks was simulated (Fig. 5C, top). The size of impulse was adjusted to match the observed
430 change in beta power in experiments. These simulations were performed using the finite model
431 with stochastic oscillators, and curves corresponding to no stimulation, most suppressive, and
432 most amplifying phases were generated. The combined effects of external stimulation and
433 intrinsic parameters constrained by bounds on both ends were consistent with the above
434 descriptions. The relative weight of each contributing factor at different synchrony levels can be
435 better understood by examining the time evolution of amplitude across three distinct levels of
436 synchrony (Fig. 5C, bottom). In a highly noisy/low coupling network, only the amplifying phase
437 caused a small upward shift in amplitude, as the already low amplitude could not be significantly
438 reduced by stimulation at the suppressing phase (Fig. 5C, left inset). Under intermediate levels of
439 coupling, far from both bounds of synchrony, a two-sided stimulation effect emerged in the
440 response (Fig. 5C, middle inset) which then disappeared under asymptotically high levels of
441 coupling due to the small instantaneous effect of stimulation (Fig. 5C, right inset).

442

443 3.4. Amplitude dependence of the response in Parkinsonian rats

444 Having refined the prediction for the magnitude of the stimulation effect as a function of synchrony
445 level, we aimed to test it by extracting the corresponding response behavior from the rat data. As
446 outlined in the Methods section, the oscillation amplitude in the model represents a normalized
447 amplitude corresponding to the level of synchrony. Therefore, to compare experimental curves
448 with theoretical predictions, one needs to first estimate the network synchrony corresponding to
449 the measured ECoG. The model fitting algorithm was employed to determine the subject-specific
450 network parameters ω_0, γ, K, D . A series of parameter recovery studies using synthetic data
451 revealed that while individual parameters could not be reliably recovered (Fig. 6-1), the resulting
452 network synchrony derived from each set of parameters was recovered with reasonable
453 confidence (Fig. 6A). As a result, rather than focusing on exact parameter values from the fitting
454 output, the corresponding network synchrony has been reported which indeed is more directly
455 relevant to the theoretical prediction. The fitting was performed to replicate three key dynamic
456 features of the signal for each animal (Fig. 6B).

457
458 Results of the model fitting implied that underlying networks producing the measured signals may
459 possess very low sustained synchrony across all animals (Fig. 6C). To highlight that different
460 combinations of network parameters can lead to the same oscillating behavior, reflected by the
461 synchrony level, the fitting algorithm was run multiple times for each subject. Although output
462 parameter values varied within each subject, all combinations consistently represented similar
463 levels of network synchrony (Fig. 6-2). The resulting model networks produced beta oscillations
464 similar to those observed in the experiments (Fig. 6D).

465

466 Next, having identified the synchrony range of interest, we investigated the experimental data
467 under two synchrony windows (block-based vs pulse-based variations) to assess whether the
468 experimental responses aligned with the response of a model operating in that regime (Fig. 6E).
469 As demonstrated in Section 3.3, low-synchrony networks are predicted to generally exhibit a
470 higher propensity for amplification compared to suppression (Fig. 5C). By closely examining the
471 blocks in the experiments, the amplitude change as a function of average amplitude prior to the
472 stimulation epoch was obtained under three conditions: reference (no stimulation applied) plus
473 the two phases achieving the highest amplification and highest suppression (Fig. 6F). At a given
474 state, the inherent noise and finite number of oscillators caused a regression to the mean in the
475 absence of stimulation. The model's response, based on best-fit parameters, aligned with the
476 experimental curves (Fig. 6G). The reference-subtracted regression lines reflected a significant
477 increase in the stimulation effect during the suppressive phase, along with a more subtle,
478 nonsignificant increase for amplification, and an overall more pronounced amplification in this
479 regime (Fig. 6-3A).

480
481 Lastly, recognizing that using averaged amplitudes over on- and off-epochs narrows the analyzed
482 synchrony window (higher and lower synchrony values are averaged out), similar amplitude
483 dependence curves were also derived based on individual stimulation pulses instead of blocks.
484 This approach accounts for a wider range of momentary synchrony levels that the network
485 experiences. It is worth noting that, while this approach uses smaller windows to calculate
486 changes in amplitude, it still combines stimulation-induced instantaneous effects with peristimulus
487 restoration governed by intrinsic parameters. The experimental pulse-based curves generally
488 exhibited similar trends to the block-based ones, except even smaller changes at the lower end
489 and a peaked trend for the amplification (Fig. 6H). This is consistent with the insight from the
490 previous section that the averaged amplitude change (Fig. 5B, top) exhibits a small dip at the low

491 end of synchrony in contrast to the instantaneous effect of pulses (Fig. 5C, top). These differences
492 were again in agreement with the curves extracted from the best-fit models (Fig. 6I). To visualize
493 the net effects of stimulation, the corresponding reference line could be subtracted from the
494 amplification and suppression lines (Fig. 6-3B).

495

496 4. Discussion

497 In this study, we elaborated on the predictions of a mathematical model based on coupled
498 oscillators regarding the effects of phase-locked stimulation on a population activity. The model
499 put forth predictions on how a neuronal population would respond to stimulation based on its
500 current state in terms of phase and level of synchrony. We utilized a previously collected dataset
501 from the study of phase-locked stimulation in rat models of PD to test those predictions.

502

503 For phase dependence, the prediction implied that the shape of ARC would follow the negative
504 of the derivative of PRC, and all except one animal exhibited response behaviors consistent with
505 the model's prediction. This key relationship, validated for the first time in this study, has been
506 investigated previously with different models. Using the Wilson-Cowan model, it has been
507 demonstrated (Duchet et al., 2020) that the phase shift between the ARC and PRC converges to
508 $\pi/2$ in the linearised model. The phase shift was however larger than $\pi/2$ in the non-linear Wilson-
509 Cowan model and in some of the data from patients with essential tremor. The predictive feature
510 of the PRC derivative was also discussed in (Wilson and Moehlis, 2014; Wilson et al., 2015)
511 through a noisy oscillators model, and in (Holt et al., 2016) with a network of conductance-based
512 neurons. On the other hand, several studies (Escobar Sanabria et al., 2020; Zaaimi et al., 2023;
513 Hebron et al., 2024) have adopted mathematical frameworks to explain the phase-dependent

514 response to stimulation. Findings of these studies have been generally consistent with the explicit
515 relationship between the ARC and PRC discussed here which is derived from a
516 phenomenological model. In addition, when evaluating the effect of phase, it must be kept in mind
517 that perfect phase tracking in practice is not feasible, especially at low amplitudes due to a lower
518 signal-to-noise ratio. Consequently, quantifying the effect of phase based on the higher amplitude
519 portions of the signal may provide a clearer perspective. Alternatively, collecting more data can
520 help mitigate this issue by averaging out the variations caused by imperfect tracking, which was
521 the case for the data used in this study. Overall, our results support the proposal that a prior
522 estimate of the PRC (such as measurements conducted for cortical (Stiefel et al., 2008),
523 subthalamic (Farries and Wilson, 2012), or pallidal neurons (Goldberg et al., 2013)) may be a
524 useful tool for determining the suppressing or amplifying phase for closed-loop DBS without a full
525 search of the parameter space (Holt et al., 2016). This approach could provide valuable guidance
526 for defining optimal stimulation parameters in clinical settings.

527

528 Amplitude dependence is a relatively unexplored aspect of the network response. Focusing solely
529 on the instantaneous effects of stimulation, the theory suggests that stimulation should become
530 ineffective at high network synchrony. However, the amplitude dependence was demonstrated to
531 be more complex as other contributing factors such as network's tendencies and bounds interact
532 with stimulation-induced changes. These interactions would lead to a decay in the effect size of
533 stimulation at both ends of the synchrony range. Moreover, distinct characteristic behaviors may
534 emerge when amplifying oscillatory activity compared to its suppression, as exemplified by the
535 stronger amplification observed in this study. This highlights the significance of determining the
536 synchrony levels of the target network beforehand if the goal is to optimize stimulation efficiency
537 based on ongoing amplitude. This could explain some of the observed differences in suppressing
538 pathological activity in patients with PD compared to those with ET (Brittain et al., 2013;

539 Schreglmann et al., 2021). We proposed here that fitting the Kuramoto model to individual
540 recordings could provide subject specific models, enabling tailored stimulation paradigms
541 according to the subject and network under study. It is also important to note that the size of
542 electrical impulses and the attainable modulation in clinical settings, which was simulated here to
543 achieve comparable changes in power, could shift the location and intensity of peaks in the
544 amplitude dependence of the response. The first-order trend, which is a general drop of the effect
545 size with increasing amplitude, has been reported in several studies (Wang et al., 2022; Hebron
546 et al., 2024), and agrees with the intuition that the stronger the synchrony of a network, the harder
547 it is to disrupt.

548

549 Beta oscillations in PD are considered an exemplar of pathological hypersynchrony. Therefore, it
550 could be considered surprising that the stimulation effect did not drop at higher amplitudes in
551 Parkinsonian rats. Importantly, however, high synchronization in the Kuramoto model represents
552 almost complete alignment of individual oscillators (e.g. Fig. 3C, right). In the Parkinsonian brain,
553 beta synchronization between neurons is massively elevated compared to healthy animals, where
554 there is very little oscillatory synchronization (Raz et al., 2001; Mallet et al., 2008b, 2008a);
555 However, if oscillators in the model represent individual neurons or ensembles of neurons in the
556 basal ganglia circuit, these pathological levels of synchronization do not approach the levels of
557 hypersynchronisation in the model. For example, in the subthalamic nucleus of Parkinsonian
558 patients the maximum proportion of individual neurons that oscillate at beta frequency and/or are
559 synchronized with cortical beta oscillations is around 60%, with a mean of 20-30% (Sharott et al.,
560 2014, 2018). In the context of developing novel approaches for DBS in PD, this suggests that
561 even highly pathophysiological levels of beta synchronization remain in the region where they
562 remain responsive to modulation by phase-dependent stimulation. It remains to be seen whether

563 this is also the case for pathophysiological activities with higher levels of synchronization, such
564 as epilepsy.

565

566 It is worth highlighting that, besides phase and amplitude, another commonly studied aspect of
567 response prediction is the frequency of oscillations and their entrainment to external rhythmic
568 stimulation—a phenomenon described by Arnold tongues. However, our analysis focused on
569 modulating a narrow band—specifically, beta oscillations—in an adaptive manner. Although an
570 average stimulation frequency can be defined in such closed-loop approaches, establishing a
571 direct connection is challenging because only one band is targeted and the stimulation strength
572 does not vary significantly.

573

574 With regards to limitations, although the model seems to capture the mean synchrony for subject-
575 specific models that reproduce the ECoG recordings, it falls short of replicating the variability of
576 oscillation amplitude observed in the animals, as seen when comparing the x-axes in Fig. 6F-I.
577 This limitation could potentially be addressed by allowing for changes in the coupling as a result
578 of synaptic plasticity, and/or using a more generalized coupled oscillators model where oscillators
579 are allowed to vary in their amplitudes. Additionally, while the model also makes predictions about
580 specific stimulation phases that lead to suppression or amplification given a specific response
581 function $Z(\theta)$, only the correlation between ARC and the PRC derivative was tested due to the
582 separate stimulation and recording sites in the experiments. Applying the developed framework
583 on experimental data where sensing and stimulation has been conducted through the same
584 electrode may facilitate further validation of the model's prediction. Moreover, the focus here was
585 placed on beta rhythms originated from basal ganglia which feature a bursty characteristic with
586 very low sustained synchrony. Testing the model through other brain rhythms and networks will

587 provide a more comprehensive image of the effects of phase-locked stimulation. Lastly,
588 alternative methods of measuring the experimental ARC and PRC could lead to slightly different
589 outcomes which is why analytical methods alone may not be sufficient to estimate network
590 synchronies.

591

592 In terms of the mechanistic explanation of the response to stimulation, it is worth noting that the
593 proposed mechanism—delayed and accelerated cycles of oscillators—can be applied at different
594 levels of abstraction, depending on the specific neural activity. While regular-spiking neurons may
595 represent the simplest interpretation of individual oscillators in some localized signals, other
596 oscillatory drives could account for broader network signals. Consequently, pinpointing the exact
597 mechanism and realization of these oscillators hinges on the scale of the measured signal and
598 may require recordings at multiple scales.

599

600 In summary, this study aimed to bridge the gap between theory and experiments by validating
601 relatively straightforward yet powerful predictions. Such mechanistic understanding of the effects
602 of stimulation could complement model free approaches like machine learning techniques to
603 design more effective stimulation policies. The findings of this study highlight the significance of
604 pinpointing the right time for stimulation, providing clinically translatable insights for optimizing
605 closed-loop strategies.

606

607 **Data and Code Accessibility**

608 No new data were generated in this study. The experimental data used here is available at
609 <http://dx.doi.org/10.5287/bodleian:9omadD7Pp>. The developed codes for mathematical modeling

610 and computational analysis would be made available on <https://github.com/Bogacz-Group> upon
611 publication.

612 References

- 613 Acebrón JA, Bonilla LL, Pérez Vicente CJ, Ritort F, Spigler R (2005) The Kuramoto model: A
614 simple paradigm for synchronization phenomena. *Rev Mod Phys* 77:137–185.
- 615 Akam T, Oren I, Mantoan L, Ferenczi E, Kullmann DM (2012) Oscillatory dynamics in the
616 hippocampus support dentate gyrus–CA3 coupling. *Nat Neurosci* 15:763–768.
- 617 Basu I, Yousefi A, Crocker B, Zelmann R, Paulk AC, Peled N, Ellard KK, Weisholtz DS,
618 Cosgrove GR, Deckersbach T, Eden UT, Eskandar EN, Dougherty DD, Cash SS, Widge
619 AS (2023) Closed-loop enhancement and neural decoding of cognitive control in
620 humans. *Nat Biomed Eng* 7:576–588.
- 621 Bergmann TO, Hartwigsen G (2021) Inferring Causality from Noninvasive Brain Stimulation in
622 Cognitive Neuroscience. *J Cogn Neurosci* 33:195–225.
- 623 Bick C, Goodfellow M, Laing CR, Martens EA (2020) Understanding the dynamics of biological
624 and neural oscillator networks through exact mean-field reductions: a review. *J Math*
625 *Neurosci* 10:9.
- 626 Breakspear M (2017) Dynamic models of large-scale brain activity. *Nat Neurosci* 20:340–352.
- 627 Brittain J-S, Probert-Smith P, Aziz TZ, Brown P (2013) Tremor suppression by rhythmic
628 transcranial current stimulation. *Curr Biol* 23:436–440.
- 629 Brown E, Moehlis J, Holmes P (2004) On the phase reduction and response dynamics of neural
630 oscillator populations. *Neural Comput* 16:673–715.
- 631 Cagnan H, Denison T, McIntyre C, Brown P (2019) Emerging technologies for improved deep
632 brain stimulation. *Nat Biotechnol* 37:1024–1033.
- 633 Cagnan H, Pedrosa D, Little S, Pogosyan A, Cheeran B, Aziz T, Green A, Fitzgerald J, Foltynie
634 T, Limousin P, Zrinzo L, Hariz M, Friston KJ, Denison T, Brown P (2017) Stimulating at
635 the right time: phase-specific deep brain stimulation. *Brain* 140:132–145.
- 636 Drobisz D, Damborská A (2019) Deep brain stimulation targets for treating depression. *Behav*
637 *Brain Res* 359:266–273.
- 638 Duchet B, Bogacz R (2024) How to design optimal brain stimulation to modulate phase-
639 amplitude coupling? *J Neural Eng* 21 Available at: [http://dx.doi.org/10.1088/1741-](http://dx.doi.org/10.1088/1741-2552/ad5b1a)
640 [2552/ad5b1a](http://dx.doi.org/10.1088/1741-2552/ad5b1a).
- 641 Duchet B, Weerasinghe G, Cagnan H, Brown P, Bick C, Bogacz R (2020) Phase-dependence
642 of response curves to deep brain stimulation and their relationship: from essential tremor

- 643 patient data to a Wilson–Cowan model. *J Math Neurosci* 10:4.
- 644 Escobar Sanabria D, Johnson LA, Yu Y, Busby Z, Nebeck S, Zhang J, Harel N, Johnson MD,
645 Molnar GF, Vitek JL (2020) Real-time suppression and amplification of frequency-
646 specific neural activity using stimulation evoked oscillations. *Brain Stimul* 13:1732–1742.
- 647 Farries MA, Wilson CJ (2012) Phase response curves of subthalamic neurons measured with
648 synaptic input and current injection. *J Neurophysiol* 108:1822–1837.
- 649 Figeo M, Mayberg H (2021) The future of personalized brain stimulation. *Nat Med* 27:196–197.
- 650 Fink CG, Murphy GG, Zochowski M, Booth V (2013) A dynamical role for acetylcholine in
651 synaptic renormalization. *PLoS Comput Biol* 9:e1002939.
- 652 Frey J, Cagle J, Johnson KA, Wong JK, Hilliard JD, Butson CR, Okun MS, de Hemptinne C
653 (2022) Past, Present, and Future of Deep Brain Stimulation: Hardware, Software,
654 Imaging, Physiology and Novel Approaches. *Front Neurol* 13:825178.
- 655 Goldberg JA, Atherton JF, Surmeier DJ (2013) Spectral reconstruction of phase response
656 curves reveals the synchronization properties of mouse globus pallidus neurons. *J*
657 *Neurophysiol* 110:2497–2506.
- 658 Gordon PC, Belardinelli P, Stenroos M, Ziemann U, Zrenner C (2022) Prefrontal theta phase-
659 dependent rTMS-induced plasticity of cortical and behavioral responses in human
660 cortex. *Brain Stimul* 15:391–402.
- 661 Guevara Erra R, Perez Velazquez JL, Rosenblum M (2017) Neural Synchronization from the
662 Perspective of Non-linear Dynamics. *Front Comput Neurosci* 11:98.
- 663 Hebron H, Lugli B, Dimitrova R, Jaramillo V, Yeh LR, Rhodes E, Grossman N, Dijk D-J, Violante
664 IR (2024) A closed-loop auditory stimulation approach selectively modulates alpha
665 oscillations and sleep onset dynamics in humans. *PLoS Biol* 22:e3002651.
- 666 Hodgkin AL, Huxley AF (1952) A quantitative description of membrane current and its
667 application to conduction and excitation in nerve. *J Physiol* 117:500–544.
- 668 Hollunder B, Rajamani N, Siddiqi SH, Finke C, Kühn AA, Mayberg HS, Fox MD, Neudorfer C,
669 Horn A (2022) Toward personalized medicine in connectomic deep brain stimulation.
670 *Prog Neurobiol* 210:102211.
- 671 Holt AB, Wilson D, Shinn M, Moehlis J, Netoff TI (2016) Phasic Burst Stimulation: A Closed-
672 Loop Approach to Tuning Deep Brain Stimulation Parameters for Parkinson’s Disease.
673 *PLoS Comput Biol* 12:e1005011.
- 674 Huerta PT, Lisman JE (1995) Bidirectional synaptic plasticity induced by a single burst during
675 cholinergic theta oscillation in CA1 in vitro. *Neuron* 15:1053–1063.
- 676 Krauss JK, Lipsman N, Aziz T, Boutet A, Brown P, Chang JW, Davidson B, Grill WM, Hariz MI,
677 Horn A, Schulder M, Mammis A, Tass PA, Volkmann J, Lozano AM (2021) Technology
678 of deep brain stimulation: current status and future directions. *Nat Rev Neurol* 17:75–87.
- 679 Krugliakova E, Karpovich A, Stieglitz L, Huwiler S, Lustenberger C, Imbach L, Bujan B,

680 Jedrysiak P, Jacomet M, Baumann CR, Fattinger S (2024) Exploring the local field
681 potential signal from the subthalamic nucleus for phase-targeted auditory stimulation in
682 Parkinson's disease. *Brain Stimul* 17:769–779.

683 Kübler D, Kroneberg D, Al-Fatly B, Schneider G-H, Ewert S, van Riesen C, Gruber D,
684 Ebersbach G, Kühn AA (2021) Determining an efficient deep brain stimulation target in
685 essential tremor - Cohort study and review of the literature. *Parkinsonism Relat Disord*
686 89:54–62.

687 Li N, Baldermann JC, Kibleur A, Treu S, Akram H, Elias GJB, Boutet A, Lozano AM, Al-Fatly B,
688 Strange B, Barcia JA, Zrinzo L, Joyce E, Chabardes S, Visser-Vandewalle V, Polosan
689 M, Kuhn J, Kühn AA, Horn A (2020) A unified connectomic target for deep brain
690 stimulation in obsessive-compulsive disorder. *Nat Commun* 11:3364.

691 Li Q, Takeuchi Y, Wang J, Gellért L, Barcsai L, Pedraza LK, Nagy AJ, Kozák G, Nakai S, Kato
692 S, Kobayashi K, Ohsawa M, Horváth G, Kékesi G, Lőrincz ML, Devinsky O, Buzsáki G,
693 Berényi A (2023) Reinstating olfactory bulb-derived limbic gamma oscillations alleviates
694 depression-like behavioral deficits in rodents. *Neuron* 111:2065-2075.e5.

695 Lozano AM, Lipsman N, Bergman H, Brown P, Chabardes S, Chang JW, Matthews K, McIntyre
696 CC, Schlaepfer TE, Schulder M, Temel Y, Volkmann J, Krauss JK (2019) Deep brain
697 stimulation: current challenges and future directions. *Nat Rev Neurol* 15:148–160.

698 Mallet N, Pogosyan A, Márton LF, Bolam JP, Brown P, Magill PJ (2008a) Parkinsonian beta
699 oscillations in the external globus pallidus and their relationship with subthalamic
700 nucleus activity. *J Neurosci* 28:14245–14258.

701 Mallet N, Pogosyan A, Sharott A, Csicsvari J, Bolam JP, Brown P, Magill PJ (2008b) Disrupted
702 dopamine transmission and the emergence of exaggerated beta oscillations in
703 subthalamic nucleus and cerebral cortex. *J Neurosci* 28:4795–4806.

704 Mansouri F, Fettes P, Schulze L, Giacobbe P, Zariffa J, Downar J (2018) A Real-Time Phase-
705 Locking System for Non-invasive Brain Stimulation. *Front Neurosci* 12:877.

706 McNamara CG, Rothwell M, Sharott A (2022) Stable, interactive modulation of neuronal
707 oscillations produced through brain-machine equilibrium. *Cell Rep* 41:111616.

708 Meidahl AC, Tinkhauser G, Herz DM, Cagnan H, Debarros J, Brown P (2017) Adaptive Deep
709 Brain Stimulation for Movement Disorders: The Long Road to Clinical Therapy. *Mov*
710 *Disord* 32:810–819.

711 Mondragón-González SL, Schreiweis C, Burguière E (2024) Closed-loop recruitment of striatal
712 interneurons prevents compulsive-like grooming behaviors. *Nat Neurosci* 27:1148–1156.

713 Netoff TI, Acker CD, Bettencourt JC, White JA (2005) Beyond two-cell networks: experimental
714 measurement of neuronal responses to multiple synaptic inputs. *J Comput Neurosci*
715 18:287–295.

716 Nieuwhof F, Toni I, Buijink AWG, van Rootselaar A-F, van de Warrenburg BPC, Helmich RC
717 (2022) Phase-locked transcranial electrical brain stimulation for tremor suppression in
718 dystonic tremor syndromes. *Clin Neurophysiol* 140:239–250.

- 719 Oswal A, Cao C, Yeh C-H, Neumann W-J, Gratwicke J, Akram H, Horn A, Li D, Zhan S, Zhang
720 C, Wang Q, Zrinzo L, Foltynie T, Limousin P, Bogacz R, Sun B, Husain M, Brown P,
721 Litvak V (2021) Neural signatures of hyperdirect pathway activity in Parkinson's disease.
722 Nat Commun 12:5185.
- 723 Ott E, Antonsen TM (2008) Low dimensional behavior of large systems of globally coupled
724 oscillators. Chaos 18:037113.
- 725 Phillips RS, Rosner I, Gittis AH, Rubin JE (2020) The effects of chloride dynamics on substantia
726 nigra pars reticulata responses to pallidal and striatal inputs. Elife 9 Available at:
727 <http://dx.doi.org/10.7554/eLife.55592>.
- 728 Polanía R, Nitsche MA, Ruff CC (2018) Studying and modifying brain function with non-invasive
729 brain stimulation. Nat Neurosci 21:174–187.
- 730 Popovych OV, Lysyansky B, Rosenblum M, Pikovsky A, Tass PA (2017) Pulsatile
731 desynchronizing delayed feedback for closed-loop deep brain stimulation. PLoS One
732 12:e0173363.
- 733 Rajamani N et al. (2024) Deep brain stimulation of symptom-specific networks in Parkinson's
734 disease. Nat Commun 15:4662.
- 735 Raz A, Frechter-Mazar V, Feingold A, Abeles M, Vaadia E, Bergman H (2001) Activity of pallidal
736 and striatal tonically active neurons is correlated in mptp-treated monkeys but not in
737 normal monkeys. J Neurosci 21:RC128.
- 738 Reis C, Arruda BS, Pogosyan A, Brown P, Cagnan H (2021) Essential tremor amplitude
739 modulation by median nerve stimulation. Sci Rep 11:17720.
- 740 Sakaguchi H (1988) Cooperative Phenomena in Coupled Oscillator Systems under External
741 Fields. Progr Theoret Phys 79:39–46.
- 742 Salimpour Y, Mills KA, Hwang BY, Anderson WS (2022) Phase- targeted stimulation modulates
743 phase-amplitude coupling in the motor cortex of the human brain. Brain Stimul 15:152–
744 163.
- 745 Scangos KW, Khambhati AN, Daly PM, Makhoul GS, Sugrue LP, Zamanian H, Liu TX, Rao VR,
746 Sellers KK, Dawes HE, Starr PA, Krystal AD, Chang EF (2021) Closed-loop
747 neuromodulation in an individual with treatment-resistant depression. Nat Med 27:1696–
748 1700.
- 749 Schreglmann SR, Wang D, Peach RL, Li J, Zhang X, Latorre A, Rhodes E, Panella E, Cassara
750 AM, Boyden ES, Barahona M, Santaniello S, Rothwell J, Bhatia KP, Grossman N (2021)
751 Non-invasive suppression of essential tremor via phase-locked disruption of its temporal
752 coherence. Nat Commun 12:363.
- 753 Sermon JJ, Olaru M, Ansó J, Cernera S, Little S, Shcherbakova M, Bogacz R, Starr PA,
754 Denison T, Duchet B (2023) Sub-harmonic entrainment of cortical gamma oscillations to
755 deep brain stimulation in Parkinson's disease: Model based predictions and validation in
756 three human subjects. Brain Stimul 16:1412–1424.
- 757 Sermon JJ, Wiest C, Tan H, Denison T, Duchet B (2024) Evoked resonant neural activity long-

- 758 term dynamics can be reproduced by a computational model with vesicle depletion.
759 Neurobiol Dis 199:106565.
- 760 Sharott A, Gulberti A, Hamel W, Köppen JA, Münchau A, Buhmann C, Pötter-Nerger M,
761 Westphal M, Gerloff C, Moll CKE, Engel AK (2018) Spatio-temporal dynamics of cortical
762 drive to human subthalamic nucleus neurons in Parkinson's disease. Neurobiol Dis
763 112:49–62.
- 764 Sharott A, Gulberti A, Zittel S, Tudor Jones AA, Fickel U, Münchau A, Köppen JA, Gerloff C,
765 Westphal M, Buhmann C, Hamel W, Engel AK, Moll CKE (2014) Activity parameters of
766 subthalamic nucleus neurons selectively predict motor symptom severity in Parkinson's
767 disease. J Neurosci 34:6273–6285.
- 768 Sharott A, McNamara C (2022) OscillTrack – Real-time neuronal oscillation tracking for closed-
769 loop stimulation. Available at: <http://dx.doi.org/10.5287/bodleian:qa9ngXrzzr> [Accessed
770 October 16, 2024].
- 771 Siegle JH, Wilson MA (2014) Enhancement of encoding and retrieval functions through theta
772 phase-specific manipulation of hippocampus. Elife 3:e03061.
- 773 Smeal RM, Ermentrout GB, White JA (2010) Phase-response curves and synchronized neural
774 networks. Philos Trans R Soc Lond B Biol Sci 365:2407–2422.
- 775 Smyth C, Anjum MF, Ravi S, Denison T, Starr P, Little S (2023) Adaptive Deep Brain
776 Stimulation for sleep stage targeting in Parkinson's disease. Brain Stimul 16:1292–1296.
- 777 Stiefel KM, Gutkin BS, Sejnowski TJ (2008) Cholinergic neuromodulation changes phase
778 response curve shape and type in cortical pyramidal neurons. PLoS One 3:e3947.
- 779 Strogatz SH (2000) From Kuramoto to Crawford: exploring the onset of synchronization in
780 populations of coupled oscillators. Physica D 143:1–20.
- 781 Strüber D, Herrmann CS (2020) Modulation of gamma oscillations as a possible therapeutic tool
782 for neuropsychiatric diseases: A review and perspective. Int J Psychophysiol 152:15–25.
- 783 Sullivan CRP, Olsen S, Widge AS (2021) Deep brain stimulation for psychiatric disorders: From
784 focal brain targets to cognitive networks. Neuroimage 225:117515.
- 785 Tinkhauser G, Pogosyan A, Little S, Beudel M, Herz DM, Tan H, Brown P (2017) The
786 modulatory effect of adaptive deep brain stimulation on beta bursts in Parkinson's
787 disease. Brain 140:1053–1067.
- 788 Velazquez JLP, Erra RG, Rosenblum M (2015) The epileptic thalamocortical network is a
789 macroscopic self-sustained oscillator: evidence from frequency-locking experiments in
790 rat brains. Sci Rep 5:8423.
- 791 Wang J, Deng B, Gao T, Wang J, Liu C (2022) Modulation of cortical oscillations by periodic
792 electrical stimulation is frequency-dependent. Commun Nonlinear Sci Numer Simul
793 110:106356.
- 794 Weerasinghe G, Duchet B, Bick C, Bogacz R (2021) Optimal closed-loop deep brain stimulation
795 using multiple independently controlled contacts. PLoS Comput Biol 17:e1009281.

796 Weerasinghe G, Duchet B, Cagnan H, Brown P, Bick C, Bogacz R (2019) Predicting the effects
797 of deep brain stimulation using a reduced coupled oscillator model. PLoS Comput Biol
798 15:e1006575.

799 Wilson D, Holt AB, Netoff TI, Moehlis J (2015) Optimal entrainment of heterogeneous noisy
800 neurons. Front Neurosci 9:192.

801 Wilson D, Moehlis J (2014) Locally optimal extracellular stimulation for chaotic
802 desynchronization of neural populations. J Comput Neurosci 37:243–257.

803 Zaaïmi B et al. (2023) Closed-loop optogenetic control of the dynamics of neural activity in non-
804 human primates. Nat Biomed Eng 7:559–575.

805 Zanos S, Rembado I, Chen D, Fetz EE (2018) Phase-Locked Stimulation during Cortical Beta
806 Oscillations Produces Bidirectional Synaptic Plasticity in Awake Monkeys. Curr Biol
807 28:2515-2526.e4.

808

809

810 **Fig. 1. The Kuramoto model of coupled oscillators to model oscillatory neural activity. A, B.** Snapshots of two
811 example sets of coupled oscillators with low (A) and high (B) synchrony levels. Dispersed oscillators result in small
812 oscillatory signal and therefore low amplitude, while packed oscillators represent large oscillation amplitude. **C.** Shift of
813 spiking in a Hodgkin Huxley model as a result of external stimulation. Depending on the stimulation time with respect
814 to the spiking cycle it can lead to phase advance (top) or delay (bottom). The dashed lines represent the spiking
815 behavior in the absence of stimulation. **D.** Schematics of the biphasic response behaviour incorporated in the model.
816 **E.** Phase response function of an individual oscillator (here, $-\sin\theta$).

817

818 **Fig. 2. Analysis of experimental data for testing theoretical predictions. A.** Summary of phase-locked experimental
819 trials conducted in Parkinsonian rats in (McNamara et al., 2022). Each trial targeted a certain phase and was divided
820 into 10-14 blocks. Two example signals, one representing stimulation at a suppressing phase (green) and one at an
821 amplifying phase (red) are shown. **B.** Schematic of block-based quantification of the phase response **C.** Schematic of
822 block-based quantification of the amplitude response. **D.** Schematic of pulse-based quantification of the amplitude
823 response. **E.** Model fitting algorithm flowchart. Dynamic features of the subject-specific experimental signal were fed
824 into an optimization solver which updates model parameters to minimize the difference between the model and
825 experimental signals.

826

827 **Fig. 3. Theoretical predictions of the network response by the Kuramoto model.** **A.** Phase and amplitude as the
828 main signal properties. Predictions are based on the network's state in terms of these properties. **B.** Model-based phase
829 dependence of the network response. ARC follows the negative derivative of PRC. Two oscillators' snapshots depict
830 extreme cases of maximum suppression (left) and maximum amplification (right). **C.** Model-based amplitude
831 dependence of the absolute change. Two oscillators' snapshots illustrate stimulation-induced changes in networks with
832 high (left) and low (right) synchrony. **D.** Combined effect of signal's phase and amplitude on the amplitude response.

833

834 **Fig. 4. Experimentally validated relationship between ARC and PRC.** **A.** Average PRC pooled across all animals.
835 The average response exhibits phase advance and delay for the population activity. **B.** Average ARC (solid line) and
836 PRC derivative (dashed line) pooled across all animals. The average amplitude response in rats is negatively correlated
837 with the derivative of the phase response. Individual response curves are presented in Figure 4-1. **C.** ARC as a function
838 of PRC derivative for 13 animals and 8 target phases. Individual correlations are presented in Figure 4-2. **D.**
839 Relationship between the correlation coefficient and the significance of phase dependence within animals. Subjects
840 (represented by circles labelled with their corresponding numbers) with more statistically significant phase dependence
841 tend to have a stronger correlation between ARC and PRC derivative.

842

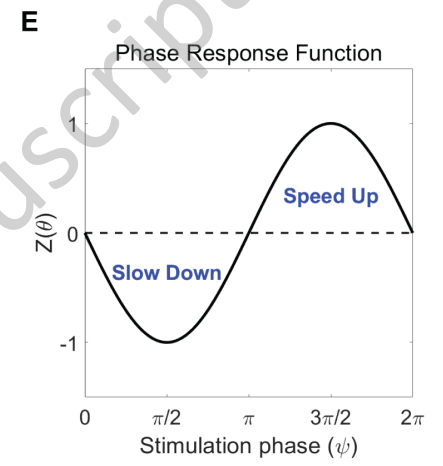
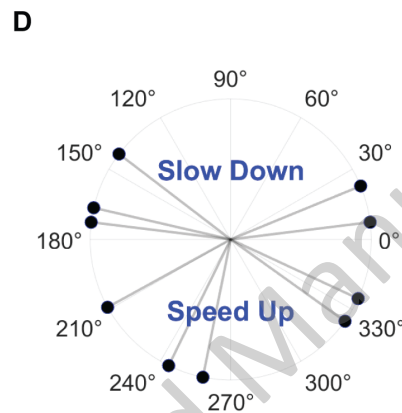
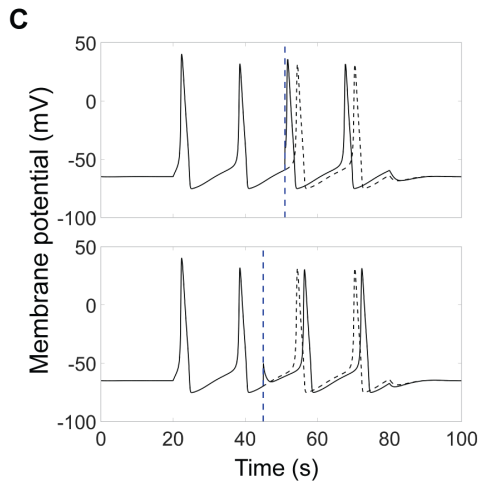
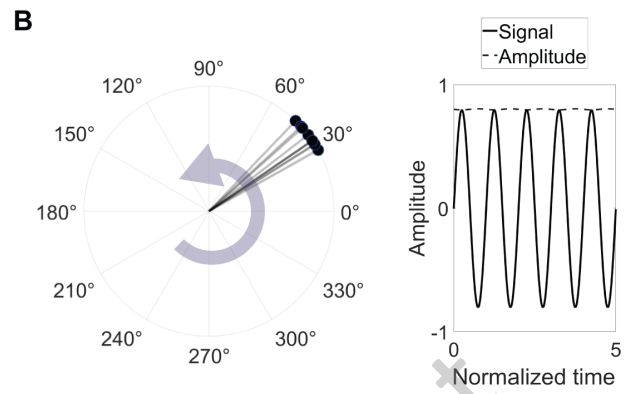
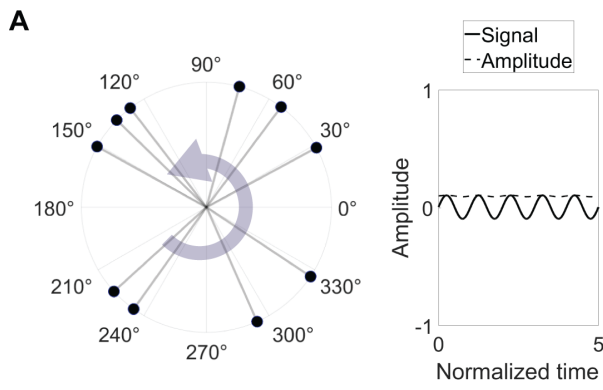
843 **Fig. 5. Contributing factors in amplitude modulation of the network response.** **A.** A seesaw analogy of a network
844 with two opposing forces and natural upper and lower bounds. External stimulation interacts with intrinsic parameters
845 to determine the synchrony level in a constrained system. **B.** Stimulation-induced instantaneous disturbance as a
846 function of oscillation amplitude. Three examples of synchrony evolution in the reduced model, each representing
847 different steady-state synchrony levels. The extent of change in network synchrony as a result of stimulation depends
848 on the size of the induced disturbance as well as network tendencies at that specific amplitude. Variations of such
849 tendencies can be visualized by the network's characteristic curve presented in Figure 5-1. **C.** Simulated block-based
850 change in oscillation amplitude as a function of amplitude prior to stimulation in the full model. Three instances of
851 amplitude evolution within a block illustrate the combined effect of stimulation-induced disturbance, intrinsic network
852 tendencies, and synchrony boundaries.

853

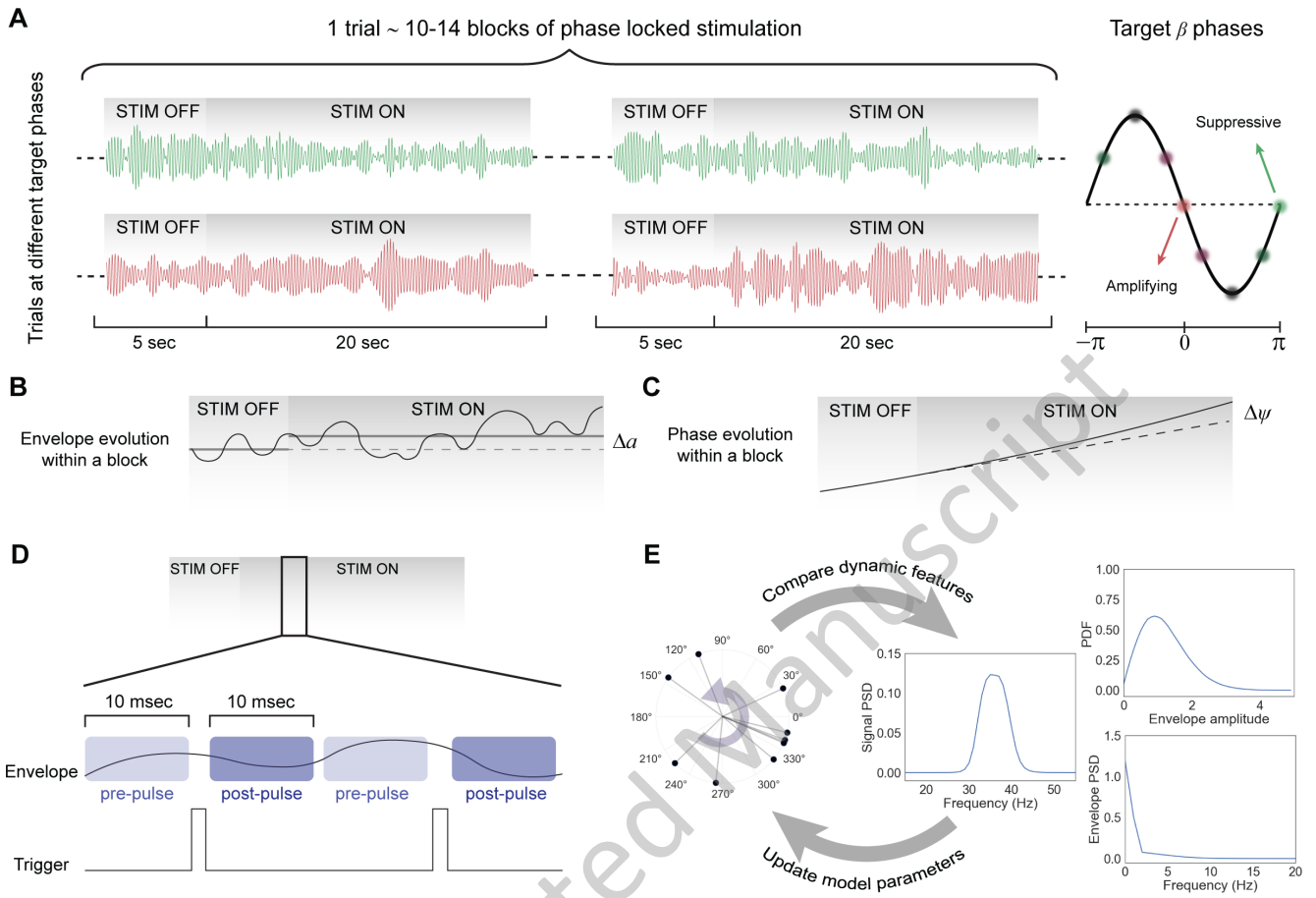
854 **Fig. 6. Network response dependence on oscillation amplitude.** **A.** Parameter recovery using synthetic data. The
855 model successfully recovers network synchrony from a set of simulated network activities. The recovery results for
856 individual parameters are shown in Figure 6-1. **B.** Results of the fitted dynamic features of the signal for an example
857 animal. The power spectral density (PSD) of the signal and its amplitude, along with the probability density function
858 (PDF) of the amplitude, were used to find the best-fitting parameters. **C.** Extracted mean synchrony for different subjects
859 obtained by fitting the Kuramoto model to experimental recordings. The dashed line represents the mean synchrony
860 when desynchronizing factors approach infinity. Details of the fitting for each subject are provided in Figure 6-2. **D.**
861 Example epochs of experimental recordings compared with simulated activity generated by the best-fit model. **E.** The
862 relevant range of synchrony in the seesaw analogy. Block-based and pulse-based analyses provide different windows
863 into the network synchrony. **F, G.** Block-based changes in amplitude as a function of pre-stimulation amplitude,
864 demonstrating stronger amplification compared to suppression in this regime. **H, I.** Pulse-based changes in amplitude
865 as a function of pre-pulse amplitude, revealing a drop in effect size at lower ends of the synchrony range through this
866 quantification method. The reference-subtracted curves for both block-based and pulse-based approaches are
867 presented in Figure 6-3.

868

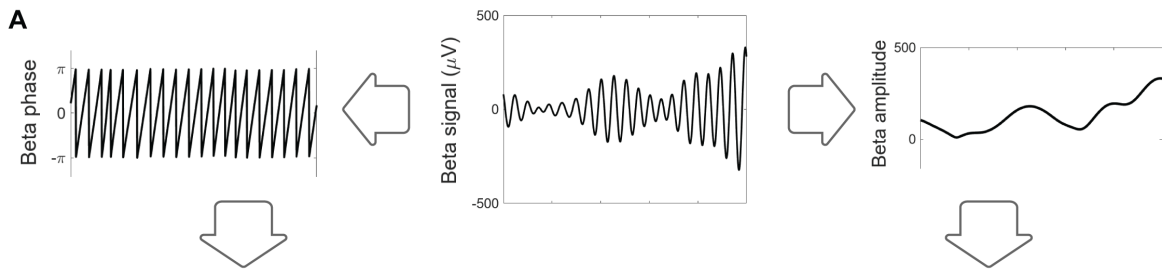
869



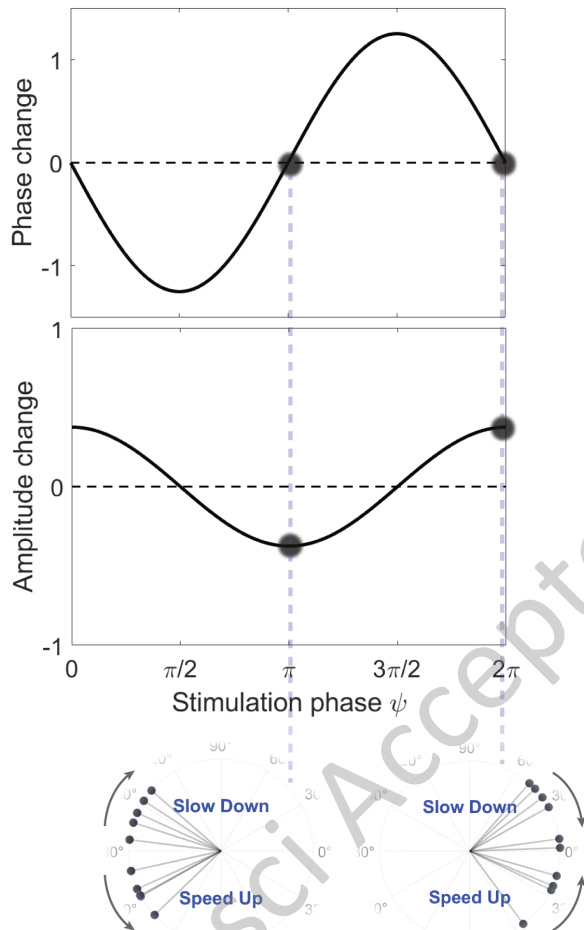
JNeurosci Accepted Manuscript



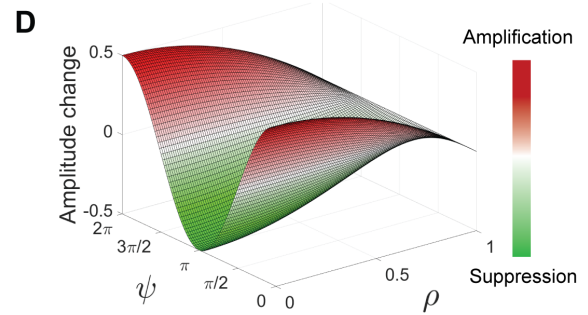
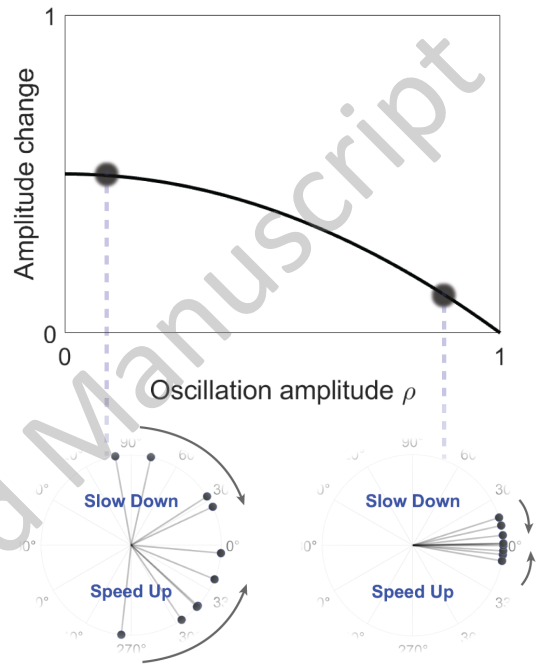
JNeurosci Accepted Manuscript

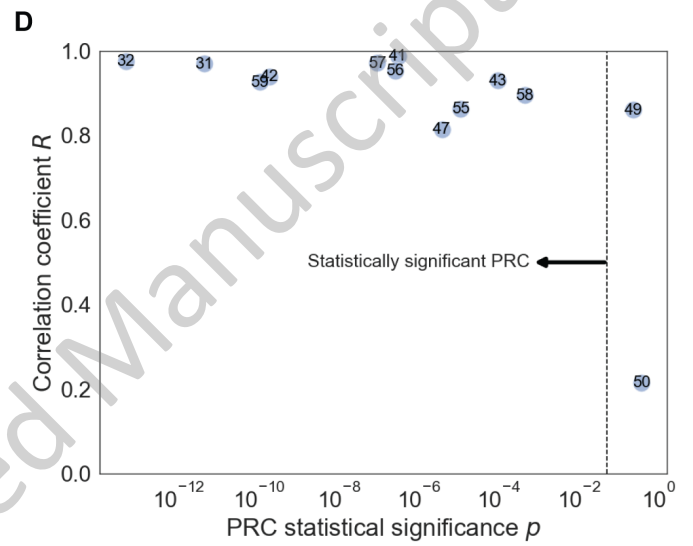
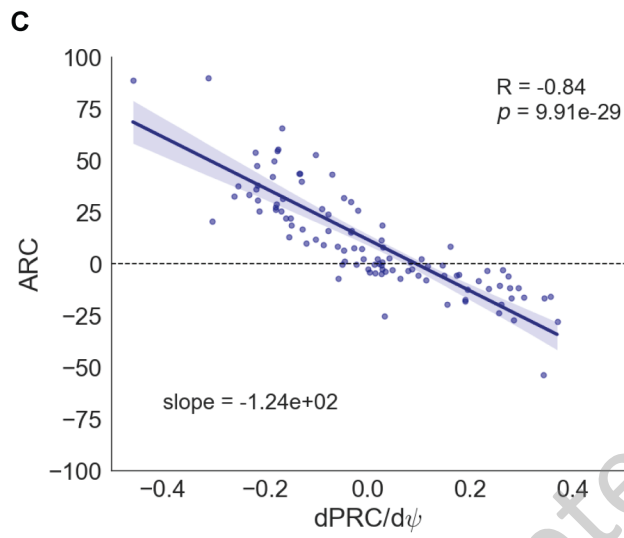
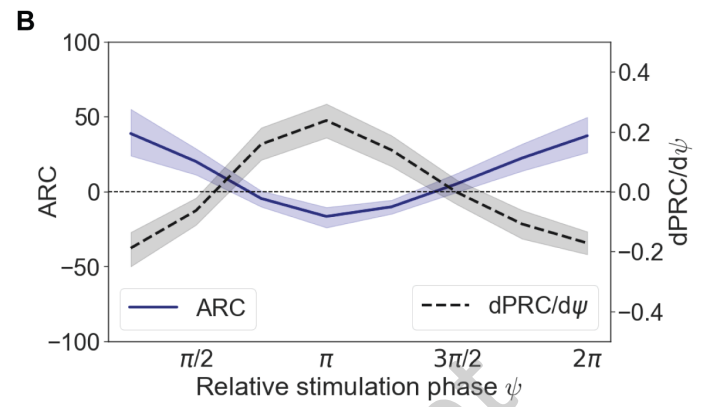
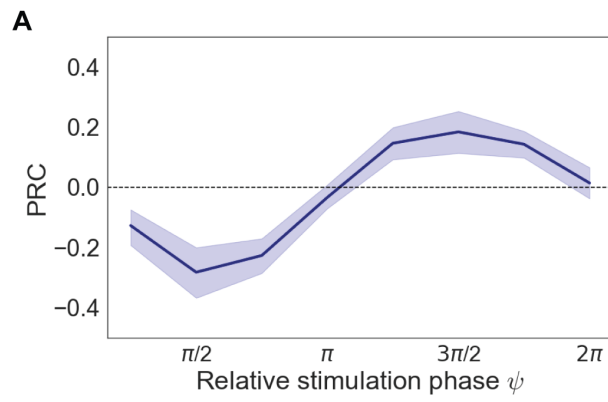


B Stimulation at an arbitrary amplitude

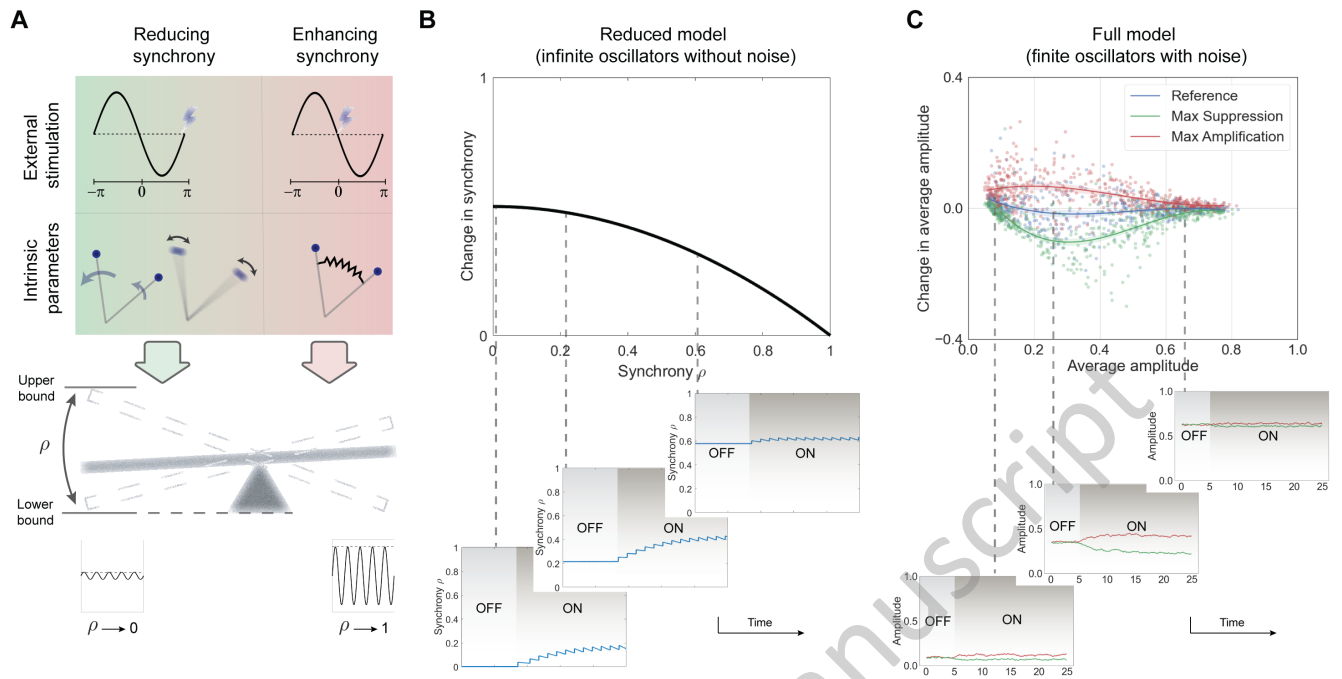


C Stimulation at an arbitrary phase





JNeurosci Accepted Manuscript



JNeurosci Accepted Manuscript

